



## Development of broad-spectrum immunoassay with monoclonal antibody to detect five eugenols and study of their molecular recognition mechanism

Lin Luo<sup>a,c,\*</sup>, Rui-Yao Kang<sup>a</sup>, Zhen-Xi He<sup>a</sup>, Bao-Zhu Jia<sup>e</sup>, Zi-Jian Chen<sup>d,\*</sup>, Hao Deng<sup>b</sup>, Zhen-Lin Xu<sup>a,c,\*</sup>

<sup>a</sup> Guangdong Provincial Key Laboratory of Food Quality and Safety, College of Food Science, South China Agricultural University, Guangzhou 510642, China

<sup>b</sup> Key Laboratory of Tropical Fruit and Vegetable Cold-chain of Hainan Province / Institute of Agro-products Processing and Design, Hainan Academy of Agricultural Sciences, Haikou 570100, China

<sup>c</sup> Heyuan Branch, Guangdong Laboratory for Lingnan Modern Agriculture, Heyuan 517000, China

<sup>d</sup> School of Food & Pharmaceutical Engineering, Zhaoqing University, Zhaoqing 526061, China

<sup>e</sup> College of Biology and Food Engineering, Guangdong University of Education, Guangzhou 510303, China

### ARTICLE INFO

#### Keywords:

Immunoassay  
Hapten  
Monoclonal antibody  
Eugenol  
Fish anesthetic

### ABSTRACT

In this study, three eugenol fragment-containing haptens were synthesized, and a monoclonal antibody (mAb) selective for five commonly-found eugenol compounds (EUGs, i.e., eugenol, isoeugenol, methyl eugenol, methyl isoeugenol, and acetyl isoeugenol) was obtained. Based on this mAb, a broad-spectrum indirect competitive ELISA for high-throughput detection of five EUGs was developed. The detection limits for eugenol, isoeugenol, methyl eugenol, methyl isoeugenol and acetyl isoeugenol in both tilapia and shrimp samples were 25.3/ 50.6 µg/kg, 0.075/0.15 µg/kg, 0.48/0.96 µg/kg, 0.16/0.32 µg/kg, and 18.16/36.32 µg/kg, respectively. The recoveries for five EUGs ranged from 80.4 to 114.0 % with a coefficient of variation less than 11.5 %. Moreover, homology modelling and molecular docking were conducted to elucidate the interactions mechanism of mAb-EUGs. The work provides a promising tool for high-throughput screening of EUGs in aquatic products, which can serve as a benchmark for designing haptens and developing immunoassays for other small molecules.

### 1. Introduction

Live fish is preferred by consumers due to their appealing taste and high nutritional content; however, the transportation and handling of live fish often subject them to stress, resulting in an elevated risk of disease and mortality, and a decline in their edible quality (Liang et al., 2023). Anesthetics can induce a sedative effect in fish, reducing their mobility, thereby lowering their vulnerability to infection and improving their survival rate (Fadillah et al., 2020). Clove oil, extracted from *Syzygium aromaticum* cloves, is predominantly made up of eugenol compounds (EUGs), such as eugenol, isoeugenol, methyl eugenol, and methyl isoeugenol (Fig. 1). Clove oil and its components all have found extensive use as fish anesthetics because of their non-specific toxicity, cost-effectiveness and high efficacy (Javahery et al., 2012). While the effectiveness of EUGs has been demonstrated in various aquaculture applications, the safety and legality of using EUGs as fish anesthetics is still in controversy. Some research indicates that exposure

to EUGs may lead to respiratory infections such as pneumonia, dermatological discomfort, and hepatic impairment (Thompson et al., 1998). The International Agency for Research on Cancer (IARC) has categorized eugenol as a Group 3 carcinogen, and toxicological information released by the National Toxicology Program reveals that methyl eugenol has the potential to elevate the risk of liver cancer (Li et al., 2015). In the United States and Canada, clove oil and its components are banned for fish anesthesia. Japan permits using eugenol in fish anesthesia, but set a maximum residue limit of 0.05 mg/kg for eugenol in aquatic products (Sun et al., 2017). In China, while EUGs are permitted as flavorings in specific food products (Huang et al., 2021; Ke et al., 2016), there are no regulations that stipulate allowable anesthetics or residue levels for aquatic products. Therefore, efficient analytical methods are essential for monitoring EUGs residues in aquatic products to mitigate the potential health impact of EUG-contaminated fish on human health.

At present, the determination of EUGs largely relies on instrumental analysis techniques, including HPLC (Thyagaraj et al., 2013; Y., 2018),

\* Corresponding authors at: Guangdong Provincial Key Laboratory of Food Quality and Safety, College of Food Science, South China Agricultural University, Guangzhou 510642, China.

E-mail addresses: [lin.luo@scau.edu.cn](mailto:lin.luo@scau.edu.cn) (L. Luo), [guangdongchenzj@163.com](mailto:guangdongchenzj@163.com) (Z.-J. Chen), [jallent@163.com](mailto:jallent@163.com) (Z.-L. Xu).

<https://doi.org/10.1016/j.fochx.2024.101255>

Received 17 November 2023; Received in revised form 13 February 2024; Accepted 25 February 2024

Available online 28 February 2024

2590-1575/© 2024 The Author(s). Published by Elsevier Ltd. This is an open access article under the CC BY-NC license (<http://creativecommons.org/licenses/by-nc/4.0/>).

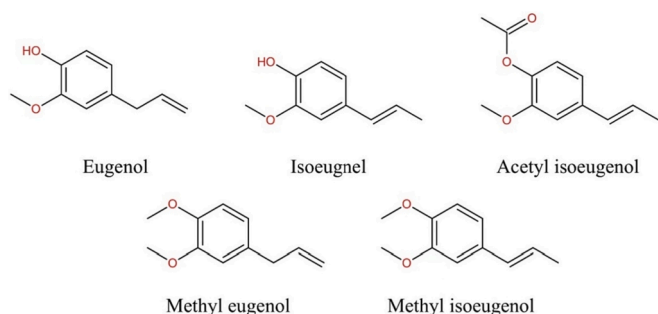


Fig. 1. Structure of Eugenol compounds.

GC-MS (Huang et al., 2021), LC-MS/MS (Ren et al., 2016), and UPLC-MS/MS (Sun et al., 2017; Zhao et al., 2017). These methods have proven to be sensitive and accurate in detecting EUGs residue levels; however, they necessitate costly instrument, highly skilled technicians, and complex sample preparation processes. Immunoassays, which rely on the specific binding between antigens and antibodies, have emerged as one of the most promising rapid detection technologies (Lin et al., 2023; Luo et al., 2022). Their simplicity, high sensitivity, specificity, and cost-effectiveness ideally compensate for the limitations of instrumental methods (X. Dong et al., 2022; Haiping et al., 2021). To date, there have been two reported immunochromatographic assays (ICAs) for EUGs. In these works, two broad-spectrum monoclonal antibodies (mAb) selective for four EUGs (i.e., eugenol, isoeugenol, methyl eugenol, and methyl isoeugenol) was elicited by using two eugenol fragment-containing haptens (termed as Eug-1 and Eug-2), and gold nanoparticle/Eu-fluorescent microspheres-based ICA were developed for rapid screening residue level of these four EUGs, respectively (Lei et al., 2023; Shen et al., 2019). However, it should be noted that ICAs are primarily suitable for qualitative or semi-quantitative detection and tend to have relatively low sensitivity. In contrast, enzyme-linked immunosorbent assay (ELISA), also as one of the most extensively applied immunoassay formats, can deliver quantitative results with high throughput and higher sensitivity under the aid of enzymatic signal amplification. Moreover, there remains room to refine the hapten design to induce mAbs with improved performance, fulfilling the need for lower detection limits.

In this work, with the aim of producing mAb with enhanced recognition performance to EUGs, three eugenol fragment-containing haptens, termed as EUG-222, EUG-250, and EUG-278, were designed and synthesized by attaching carboxylic spacer arms of two, four, and six carbon lengths, respectively, to the hydroxyl group position of eugenol (Fig. 2). A monoclonal antibody (termed as anti-EUGs) showed broad-spectrum recognition to commonly-found five EUGs with improved affinity was produced. Based on this anti-EUGs mAb, a broad-spectrum indirect competitive enzyme-linked immunosorbent assay (ic-ELISA)

was developed for high-throughput screening five EUGs residue in edible aquaculture fish. Additionally, to explain the different affinities of the mAb with five EUGs, homology modelling and molecular docking were conducted to study the interactions between the variable region of mAb and EUGs compound. These findings improve our understanding of immunoassay results and offer direction for the continued molecular revolution for the development of antibodies with better performance.

## 2. Materials and methods

### 2.1. Reagents and apparatus

Eugenol, isoeugenol, eugenol methyl eugenol, methyl isoeugenol, acetyl isoeugenol, and other structural analogs were purchased from Tanmo Quality Inspection Technology Co., Ltd (Beijing, China). Ethyl 6-bromohexanoate, ethyl 4-bromobutylate, ethyl bromoacetate, *N,N*-Diisopropylethylamine (DIEA), and *O*-Benzotriazole-*N,N,N',N'*-tetramethyl-uronium-hexafluorophosphate (HBTU) were obtained from Macklin Biochemical Co., Ltd. (Shanghai, China). Concentrated hydrochloric acid (HCl) was supplied by Sinopharm Chemical Reagent (Beijing, China). Lactoferrin (LF) and ovalbumin (OVA), hypoxanthine aminopterin thymidine (HAT), hypoxanthine thymidine (HT), complete and incomplete Freund's adjuvant, polyethylene glycol (PEG) 1500 were procured from Sigma-Aldrich (Shanghai, China). Cell culture plates were obtained from Corning Life Sciences (New York, USA). HRP-conjugated goat anti-mouse IgG (secondary antibody) was purchased from Qixiang Biological Co., Ltd. (Guangzhou, China). Fetal Bovine Serum (FBS) was supplied from ExCell Bio—company (Taicang, China). Lithium hydroxide (LiOH), sodium hydroxide (NaOH), sodium chloride (NaCl), potassium chloride (KCl), sodium bicarbonate, sodium carbonate, potassium carbonate, acetonitrile, ethanol, potassium phosphate monobasic, *N,N*-dimethylformamide (DMF), Tween-20, methanol (MeOH) and ethyl acetate were obtained from Damao Chemical Reagent Co., Ltd. (Tianjin, China). 96-Well polystyrene microplates were purchased from Xiamen Yijiamei Industrial Co. Ltd. (Xiamen, China). RPMI 1640 medium, penicillin-streptomycin solution, and pierce™ rapid antibody isotyping kit-mouse were obtained from Thermo Fisher (Shanghai, China). Female Bal b/c mice were supplied by Vital River Laboratory Animal Technology (Beijing, China) and raised at South China Agriculture University Animal Centre (license: SYXK (Yue) 2022-0136). The animal experiment was conducted in a laboratory with a license for experiment animals, which conformed to the welfare principle (ethical approval number: 2021B119). All other reagents were of analytical reagent grade or higher purity.

The antibody concentration and the antigens' conjugating resultant were detected using a NanoDrop 2000c spectrophotometer (Thermo Fisher, Shanghai, China). The ELISA plates were washed in a Well-wash™ microplate washer (Thermo Fisher, Shanghai, China). Absorbance was measured at a wavelength of 450 nm using a Multiskan MK3

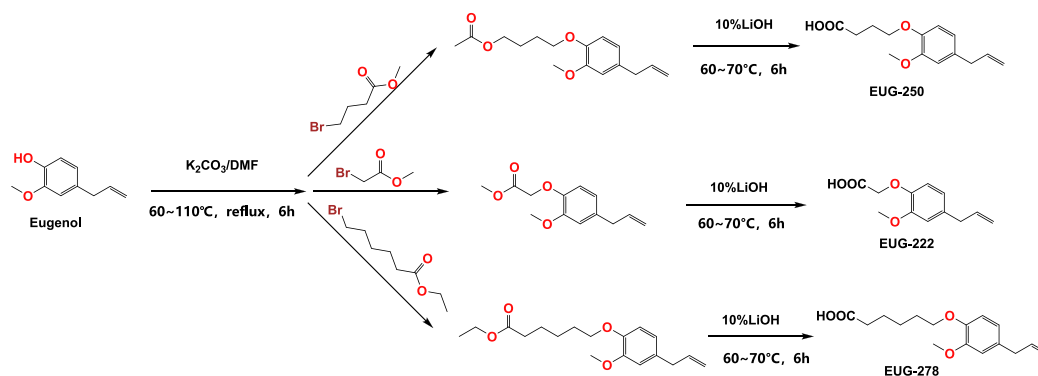


Fig. 2. Synthetic route for hapten (a) EUG-250, (b) EUG-222, (c) EUG-278.

microplate reader (Thermo Fisher, Shanghai, China). Nuclear magnetic resonance (NMR) spectra were recorded with a DRX-600 NMR spectrometer (Bruker, Rheinstetten, Germany).

## 2.2. Synthesis of haptens

Three haptens, termed as EUG-222, EUG-250, and EUG-278, were designed and synthesized by introducing three different carboxylic spacer arms at the hydroxyl group site of eugenol, respectively. Synthetic pathway displayed in Fig. 2. ESI-MS and NMR spectra of these three haptens are presented in the Supplementary Materials (Fig. S1–S6).

**Synthesis of hapten EUG-222.** 1.5 mL (0.01 mol) of eugenol, 1.2 mL (0.01 mol) of ethyl bromoacetate and 2.76 g (0.02 mol) of potassium carbonate were added to 15 mL of DMF under stirring, which was then refluxed at 110 °C for 6 h. After cooling to temperature, 50 mL of water was added to the reaction mixture, which was then extracted with ethyl acetate three times. The combined organic layer was washed with brine (25 mL), dried with Na<sub>2</sub>SO<sub>4</sub>, and evaporated in vacuo to give a colorless oil. The resulting colorless oil was dissolved in 10 mL of lithium hydroxide solution (10 %) with the addition of 5 mL of methanol. The mixture was allowed to react at 70 °C for 6 h. After cooling to room temperature, the resulting mixture solution was acidified by HCl (6 mol/L) and extracted with ethyl acetate three times. The combined organic phase was dried by anhydrous Na<sub>2</sub>SO<sub>4</sub>, and concentrated by rotary evaporation, forming a brownish-yellow solid product, which is the hapten EUG-222. ESI-MS (positive) *m/z*:223.2 [M + H]<sup>+</sup>; ESI-MS (positive) *m/z*:221.2 [M–H]<sup>–</sup>; <sup>1</sup>H NMR (600 MHz, MeOD) δ 6.88–6.79 (m, 2H, aromatic H), 6.69 (dd, 1H, aromatic H), 5.94 (ddt, 1H, –CH = ), 5.04 (m, 2H, –CH<sub>2</sub>), 4.61 (s, 2H, –CH<sub>2</sub>–O), 3.82 (s, 3H, CH<sub>3</sub>–O), 3.31 (m, 2H, –CH<sub>2</sub>–).

**Synthesis of haptens EUG-250 and EUG-278.** Synthesis of haptens EUG-250 and EUG-278 were similar to that of EUG-222, in which ethyl bromoacetate was replaced by ethyl 4-bromobutyrate and ethyl 6-bromocaproate, respectively. EUG-250: ESI-MS (positive) *m/z*:251 [M + H]<sup>+</sup>; ESI-MS (positive) *m/z*:249.1 [M–H]<sup>–</sup>; <sup>1</sup>H NMR (600 MHz, MeOD) δ 6.92–6.65 (m, 3H, aromatic H), 5.94 (m, 1H, –CH = ), 5.03 (m, 2H, = CH<sub>2</sub>), 3.99 (t, 2H, –CH<sub>2</sub>–O), 3.81 (s, 3H, CH<sub>3</sub>–O), 3.30 (m, 2H, –CH<sub>2</sub>–C = ), 2.50 (t, 2H, –CH<sub>2</sub>–), 2.03 (m, 2H, –CH<sub>2</sub>–CO). EUG-278: ESI-MS (positive) *m/z*:279.1 [M + H]<sup>+</sup>; ESI-MS (positive) *m/z*:277.2 [M–H]<sup>–</sup>; <sup>1</sup>H NMR (600 MHz, CDCl<sub>3</sub>) δ 6.91–6.60 (m, 3H, aromatic H), 5.96 (ddt, 1H, –CH = ), 5.05 (m, 2H, = CH<sub>2</sub>), 3.98 (m, 2H, CH<sub>2</sub>–O), 3.85 (s, 3H, CH<sub>3</sub>–O), 3.33 (d, 2H, –CH<sub>2</sub>–C = ), 2.38 (dd, 2H, CH<sub>2</sub>–CO), 1.86 (m, 2H, –CH<sub>2</sub>–), 1.71 (m, 2H, –CH<sub>2</sub>–), 1.53 (m, 2H, –CH<sub>2</sub>–).

## 2.3. Preparation of artificial antigens and anti-EUGs mAb

Active ester method was used to conjugate these three haptens to LF and OVA to prepare immunogens (EUG-222-LF; EUG-250-LF; EUG-278-LF) and coating antigens (EUG-222-OVA; EUG-250-OVA; EUG-278-OVA), respectively. Briefly, each hapten (0.1 mmol) was first dissolved in 0.3 mL of dimethylformamide (DMF), followed by the addition of DIEA (0.12 mmol) and HBTU (0.12 mmol). This mixture was then stirred at room temperature for 4 h. Subsequently, it was added dropwise to a 2.0 mL solution of protein (either 20 mg of LF or 20 mg of OVA), which had been prepared in CB buffer (0.05 M, pH 9.6). The resulting mixture was left to stir overnight at room temperature. Afterward, the mixture underwent dialysis using a semipermeable membrane against phosphate-buffered saline (PBS) (0.01 M, pH 7.4) for three days to remove any unreacted haptens and by-products from the conjugation reaction. The resulting conjugate solution was then stored at a frozen temperature of –20 °C until needed. The resultant hapten-protein conjugates were characterized using UV–visible absorption spectroscopy.

All the female Balb/c mice were raised in the Animal Center of South China Agricultural University (license: SYXK (Yue) 2022–0136). All the animal experiments were conducted by China's Laboratory Animal

Protection Law and Management Law and were approved by the Laboratory Animal Care Institution of South China Agricultural University, Guangzhou, China (ethics approval number: 2021B119). Nine female BALB/c mice were randomly assigned to three groups and each was immunized with one of three immunogens (EUG-222-LF, EUG-250-LF, EUG-278-LF). The immunization protocol and the process for generating monoclonal antibodies (mAbs) against EUGs followed the procedures outlined in our previous work (Luo et al., 2018). Positive hybridoma cell lines were identified using indirect competitive ELISA (ic-ELISA) and subsequently subcloned through five rounds of limiting dilution. The resulting mAbs were purified using commercially available protein G resin and stored at –20 °C. The antibody affinity was determined by saturation concentration method. Added 100 μL of a series of concentration of antibody into the coated 96-well ELISA plate and analysis by ic-ELISA. Established the concentration curve of antigen–antibody complex. K<sub>d</sub> was defined as antibody concentration when the concentration of antigen–antibody complex accounted for half of the antigen concentration. K<sub>a</sub> was the inverse of K<sub>d</sub>.

## 2.4. Protocol of ic-ELISA for EUGs detection

The procedures of ic-ELISA were performed as previously described (Luo et al., 2019). Briefly, each well of the microplates was coated with 100 μL of the coating antigen at a concentration of 500 ng/mL and left to incubate for 12 h at 4 °C. Following two washes with wash buffer, the wells were blocked with 120 μL per well of 5 % skim milk dissolved in PBST at 37 °C for a duration of 3 h. After the blocking solution was removed, 50 μL of varying concentrations of EUGs standards or the sample solution were added to each well, along with 50 μL of anti-EUGs mAb, in sequence. The wells were then incubated for 40 min at 37 °C. Subsequently, the plate underwent five wash cycles before the addition of 100 μL of horseradish peroxidase (HRP)-conjugated goat anti-mouse IgG to each well, which was then incubated for an additional 30 min at 37 °C. After another five washes, 100 μL of chromogenic substrate is added and incubated at 37 °C for 10 min. Finally, the reaction is terminated by 50 μL of H<sub>2</sub>SO<sub>4</sub> (10 %), and the absorbance at 450 nm is measured using a microplate reader. Calibration curves were constructed by plotting the normalized signal (B/B<sub>0</sub>, Y axis) against the logarithm of the analyte concentration (X axis). In this context, B<sub>0</sub> is the average absorbance of the wells without the competitor, while B is the mean absorbance of the wells when the competitor is present. To fit the sigmoidal curve, a four-parameter logistic equation was utilized, and this curve fitting was carried out using Origin 8.6 software (Origin Lab Corp., Northampton, MA). The equation is as follows:

$$Y = \frac{(A - D)}{1 + \left(\frac{X}{C}\right)^E} + D$$

In this context, A represents the highest possible response on the upper end of the curve, while D indicates the lowest response on the lower end. The concentration of the inhibitor required to achieve 50 % of the maximum inhibition is denoted by C, which is the half inhibitory concentration (IC<sub>50</sub>). The parameter E refers to the slope of the sigmoidal curve. The limit of detection (LOD) is established at the analyte concentration that results in a 10 % inhibition level (IC<sub>10</sub>). The dynamic linear range is determined between the points on the curve where the inhibition is 20 % and 80 %, corresponding to the concentrations between IC<sub>20</sub> and IC<sub>80</sub>.

## 2.5. Cross-reactivities

The specificity and binding affinity of the mAbs to EUGs and analogs were evaluated using indirect competitive ELISA (ic-ELISA). The cross-reactivity (CR) with a range of structurally or functionally related EUGs analogs were determined using the subsequent formula: CR =

$$[(IC_{50} \text{ eugenol}) / (IC_{50} \text{ analog})] \times 100\%.$$

## 2.6. Sample pretreatment

The tilapia fish and shrimp sample were obtained from local market in South China Agricultural University, and were all confirmed eugenols-negative by GC-MS. (parameters of the GC-MS/MS were listed in Table S1-S5) Tilapia fish and shrimp were finely minced and thoroughly mixed prior to taking samples. A 2 g sample was placed into a 10 mL centrifuge tube containing 1 g of anhydrous sodium sulfate and 5 mL of acetonitrile. The tube was vortexed for 1 min and then ultrasonicated for 10 min. After ultrasonication, the mixture was centrifuged at 9500 rpm for 3 min. The clear supernatant was decanted into another 10 mL centrifuge tube. The extraction process was repeated on the sample with an additional 5 mL of acetonitrile. The supernatants from both extractions were then combined and passed through a 0.22  $\mu\text{m}$  membrane filter before being concentrated to dryness under a stream of nitrogen at 45 °C. The resultant residue was reconstituted in 2.0 mL of PBS (0.01 M, pH 7.4). For tilapia fish sample, the extract solution was further diluted 8-fold in PBS (0.01 M, pH 7.4) for the analysis by ic-ELISA, while a 16-fold dilution was necessary for shrimp sample.

## 2.7. Homology modeling and molecular simulations

The VH and VL gene fragments of anti-EUGs mAb was cloned from hybridoma cells according to the method in previous work (J. Dong et al., 2021). The amino acid sequences of the VH and VL were translated using the DNAMAN software (version 5.2.2). The three-dimensional model of VH and VL were constructed via modeling using the alpha-fold 2.0. Afterward, the Fv model was constructed using an antibody template (PDBID: 1IGY) by Pymol (version 2.4.0a0, open-source). The obtained Fv 3D structure was evaluated using via Ramachandran plots on the SAVES online database (<https://saves.mbi.ucla.edu>). The molecular structures of EUGs (ligands) were acquired from the ZINC database (<http://zinc.docking.org/>). Docking simulations were conducted using LeadIT 2.1.8 software (<https://www.biosolveit.de/LeadIT/>) via a hybrid approach combining Enthalpy and Entropy for ligand binding settings, while leaving the other parameters at their default values. The energy minimization of the Fv model for dynamic simulation was conducted using the GROMACS 2021.3 software (<http://www.gromacs.org/>). The SPC model was chosen for the solvent model with a minimum distance requirement of 1.0 Å from the cube's edge. To prepare for production molecular dynamics (MD) simulations, the structure's energy was minimized using 5,000,000 optimization runs, employing a time step of 2 fs (fs) for a total simulation time of 10 ns (ns). The simulation was conducted at a constant temperature of 310 K.

## 3. Results and discussion

### 3.1. Characterization of hapten and antigen

The performance of antibodies in binding to small molecules is widely recognized as being heavily dependent on the structure of the immunizing hapten (Luo et al., 2017). Typically, an ideal hapten is considered to be one that retains as much of the target molecule's structure as possible after being conjugated to a carrier protein (Liang et al., 2023). Previously, Shen et al designed and synthesized eugenol-containing hapten by introducing a four-carbon-length carboxylic spacer arm at the hydroxyl group site of eugenol, and a broad-spectrum mAb selective for four EUGs was obtained (Shen et al., 2019). Nevertheless, it has been widely acknowledged that the length of hapten spacer arm showed significant influence on the antibody response and immunoassay development (Bai et al., 2023; Luo et al., 2017). In this study, with the aim of producing mAb with enhanced recognition performance to EUGs, three haptens were synthesized, named EUG-222, EUG-250, and EUG-278, were designed and synthesized by attaching

carboxylic spacer arms of two, four, and six carbon lengths, respectively, to the hydroxyl group position of eugenol. The successful synthesis of these haptens was confirmed through Electrospray Ionization Mass Spectrometry (ESI-MS) and Nuclear Magnetic Resonance (NMR) spectroscopy (Fig. S1-S6). The UV-vis spectroscopy analysis of the hapten-protein conjugates, as shown in Fig. S7, reveals a noticeable shift in the characteristic absorption bands of the carrier proteins, lactoferrin (LF) and ovalbumin (OVA), upon conjugation with the haptens, indicating that the synthesis of these artificial antigens was successfully achieved.

### 3.2. Characterization of anti-EUGs mAb

The immunization results showed that the antisera obtained from mouse immunized with the hapten EUG-222 showed good the best binding affinity to eugenol (Table S6-S8). Therefore, mice immunized with EUG-222-LF were chosen as spleen cell donors for cell fusion to prepare monoclonal antibodies. Spleen cells obtained from mice were fused with SP2/0 myeloma cells using polyethylene glycol (PEG). Through a series of five subcloning steps, a cell line that produced mAb targeting eugenol (anti-EUG mAb) was successfully established. Subsequently, after preparing ascites and purifying the antibodies, their purity was assessed using SDS-PAGE electrophoresis. As depicted in Fig. 3A, the electrophoresis results displayed two distinct protein bands, with approximate molecular weights of around 25 kDa and 55 kDa, corresponding to the light and heavy chains of the mAb, respectively. This indicates a high-purity anti-EUG mAb was obtained. The subtype of the mAb was identified as IgG1 (Fig. 3B). The affinity constant  $K_d$  of the mAb to eugenol was determined to be  $7.7 \times 10^{-10}$  mol/L and the dissociation constant  $K_a$  was  $1.3 \times 10^9$  L/mol (Fig. 3C).

### 3.3. Development of the ic-ELISA for EUGs

The sensitivity of the ic-ELISA is greatly affected by the concentrations of the primary antibody and the coating antigen. Multiple concentration combinations of the coating antigen and the anti-EUGs mAb were evaluated by checkerboard titration method. As shown in Table S9, the highest sensitivity was achieved using a coating antigen concentration of 0.5  $\mu\text{g}/\text{mL}$ , an antibody concentration of 0.25  $\mu\text{g}/\text{mL}$  with an ic-ELISA inhibition rate of 77 % when using 100 ng/mL of eugenol as the competitor. Under the optimal conditions, calibration curves were plotted for five EUGs by correlating B/B<sub>0</sub> to their concentrations, from which the half-maximal inhibitory concentration (IC<sub>50</sub>) values, LOD (IC<sub>10</sub>) and linear range (IC<sub>20</sub>-IC<sub>80</sub>) were determined (Fig. 4). The ic-ELISA exhibits a IC<sub>50</sub> of 38.19 ng/mL with LOD of 3.16 ng/mL and a linear range of 7.92-184.05 ng/mL for eugenol; an IC<sub>50</sub> of 0.15 ng/mL, a linear range of 0.026-0.865 ng/mL, and a LOD of 9.35 pg/mL for isoeugenol; an IC<sub>50</sub> of 0.80 ng/mL, a linear range of 0.15-4.30 ng/mL, and a LOD of 0.06 ng/mL for methyl eugenol; an IC<sub>50</sub> of 0.44 ng/mL, a linear range of 0.06-3.04 ng/mL, and a LOD of 0.02 ng/mL for methyl isoeugenol; an IC<sub>50</sub> of 21.93 ng/mL, a linear range of 5.24-91.76 ng/mL, and a LOD of 2.27 ng/mL for acetyl isoeugenol (in buffer solution).

The CRs with other non-EUGs compounds including Vanillylideneacetone (2.0 %), 4-Ethyl-2-methoxyphenol (8.7 %) and function-related anesthetics (less than 0.1 %), were negligible (Table 1). These results indicate the good broad-specificity of the ic-ELISA for commonly-found EUGs. Moreover, compared with previously reported mAb against EUGs (Table S10), this anti-EUG mAb showed not only much higher affinity to isoeugenol, methyl eugenol, methyl isoeugenol, but also broader recognition spectrum to EUGs (five EUGs versus four EUGs), though relatively lower affinity to eugenol than that of 1B5 mAb (IC<sub>50</sub> = 9.23 ng/mL) was observed.

### 3.4. Recovery test in spiked samples

Before analyzing real samples, it is crucial to evaluate the sample

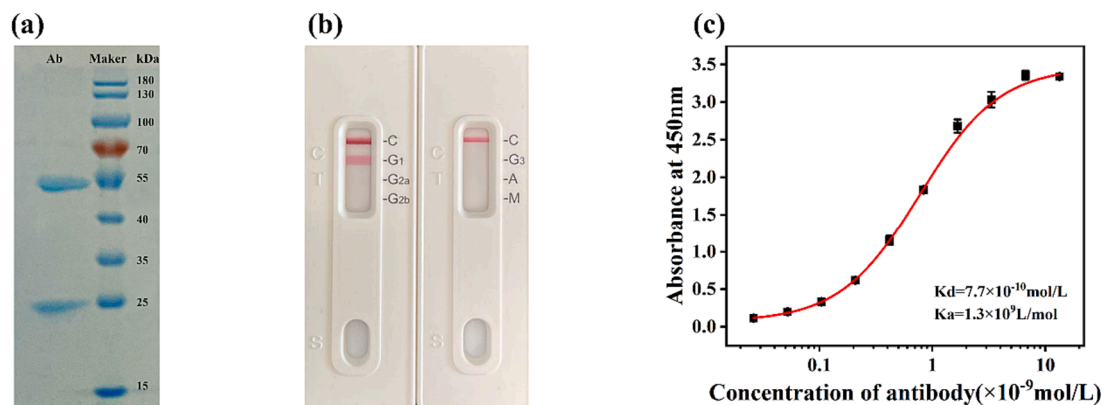


Fig. 3. The result of SDS-PAGE (a). The subtype of anti-EUGs mAb (b). Affinity constant curves of anti-EUGs mAb to eugenol (c).

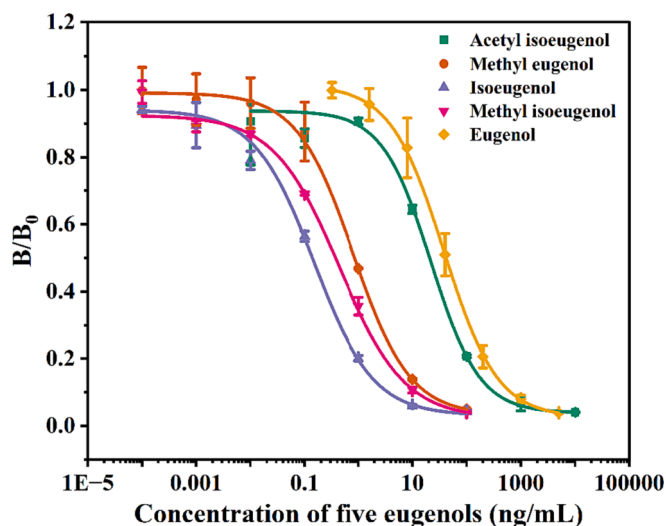


Fig. 4. Calibration curves for five eugenol compounds.

matrix effect on the accuracy of the assay. In this study, matrix-based calibration curves were constructed by using matrix solution diluted 2, 4, 8, 16, and 32 times by working buffer. Typically, with the increase in dilution factor, the slope of the matrix-based calibration curve ( $A_{max}/IC_{50}$ , where  $A_{max}$  represents the absorbance value in the absence of nitrite) gradually approached that of the buffer-based calibration curve, indicating a diminishing effect of the matrix. As depicted in Fig. S8, an 8-fold dilution of the tilapia sample and a 16-fold dilution of the shrimp sample were necessary to eliminate matrix effects, respectively. This was evident as the corresponding  $A_{max}/IC_{50}$  values increased to levels closely approximating those of the PBS-based calibration curve. Therefore, taking the sample dilution into consideration, the LODs for eugenol, isoeugenol, methyl eugenol, methyl isoeugenol and acetyl isoeugenol in both tilapia and shrimp samples were 25.3/ 50.6  $\mu\text{g}/\text{kg}$ , 0.075/0.15  $\mu\text{g}/\text{kg}$ , 0.48/0.96  $\mu\text{g}/\text{kg}$ , 0.16/0.32  $\mu\text{g}/\text{kg}$ , and 18.16/36.32  $\mu\text{g}/\text{kg}$ , respectively. In spiked tilapia and shrimp samples, five eugenol compounds were separately added at 10, 50, and 100  $\mu\text{g}/\text{kg}$ , and the recovery for eugenol compounds in tilapia samples was ranging from 80.4 % to 114.0 % with CVs below 11.5 % (Table S11). For spiked shrimp samples, the recovery was between 81.8 % and 110.7 % with CVs less than 9.5 % (Table S12). These results demonstrate that this method is with good accuracy and reliability, making it a promising tool for routine EUGs residues screening in aquatic products.

### 3.5. Investigation of recognition mechanism

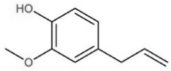
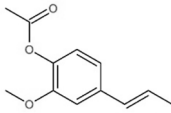
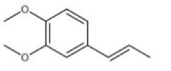
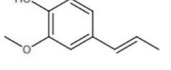
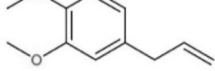
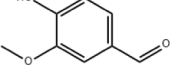
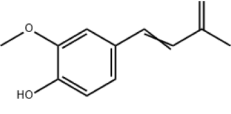
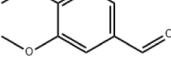
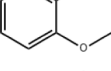
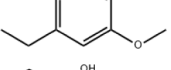
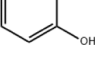
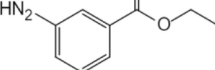
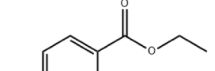
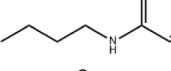
These aforementioned results indicate the good broad-spectrum recognition ability of this mAb to commonly-found EUGs. However, this anti-EUG mAb displayed much higher binding affinity to isoeugenol ( $IC_{50} = 0.15$  ng/mL), methyl isoeugenol ( $IC_{50} = 0.44$  ng/mL) and methyl eugenol ( $IC_{50} = 0.80$  ng/mL) than eugenol ( $IC_{50} = 38.19$  ng/mL) though the immunizing hapten was obtained by the modification on the basis of eugenol's structure. To explain the unexpected recognition phenomenon, homology modeling and molecular docking was conducted to investigate the molecular interaction between the Fv of this mAb and EUGs.

RNA was successfully extracted from hybridoma cells, followed by reverse transcription and PCR cloning to obtain VH and VL gene fragments. Subsequently, the corresponding amino acid sequence of VH and VL was obtained using DNAMAN software (Table S13). The three-dimensional model of VH and VL was constructed via modeling using the alphafold 2.0. Using an antibody model (PDB ID: 11GY) as a template, a 3D model of the Fv was obtained by aligning the heavy and light chains to the Fv template with the PyMOL software (Fig. 5A). The simple merging of the Fv model caused atomic overlaps and other unreasonable conformations, thus molecular dynamics were needed to correct these unreasonable conformations. The RMSD (root-mean-square deviation) in Fig. 5B indicates that after a 10 ns simulation, the model has reached an equilibrium state. Subsequently, the Ramachandran plot was used to evaluate the rationality of the equilibrium Fv model structure. The results show that more than 90 % of the amino acid residues are located in the reasonable and additionally reasonable regions (Fig. 5C and D), indicating that its structure is rational and can be used for the subsequent simulation docking.

The docking results of the Fv with eugenol are shown in Fig. 6A1 and A2, where eugenol is located in the active pocket of Fv. Its butenyl group extends into the bottom of the active pocket, forming hydrophobic interactions with Tyr49(L) of the light chain, while the phenyl group of eugenol faces outward from the pocket. The hydroxyl and methoxy groups on the phenyl ring each form a 1.9 Å hydrogen bond with Arg50 (L) of the light chain. Additionally, the phenyl ring forms hydrophobic interactions with Tyr100(H) of the heavy chain and His91(L) of the light chain, with Tyr100(H) being parallel to the phenyl group of eugenol, forming  $\pi$ - $\pi$  interactions, which further strengthen the affinity between the antibody and the ligand.

Isoeugenol has the highest binding activity with the mAb. As seen from Fig. 6B1 and 6B2, isoeugenol penetrates deeply into the CDR pocket and forms strong hydrophobic interactions with aromatic residues such as Tyr32(H), Tyr100(H), and Tyr49(L). From Fig. 6B2, it is evident that the antibody forms the greatest number (four in total) of hydrogen bonds with isoeugenol, where the hydroxyl and methoxy groups on the phenyl ring each form three hydrogen bonds with Arg50

**Table 1**  
Cross-reactivity of the ic-ELISA with EUGs and their analogs.

Compound	Structure	IC <sub>50</sub> (ng/mL)	CR (%)
Eugenol		38.19	100
Acetyl isoeugenol		21.93	174.1
Methyl isoeugenol		0.44	8679.5
Isoeugenol		0.15	25460.0
Methyl eugenol		0.80	4773.8
Vanillin		>10000	<0.4
Vanillylideneacetone		1914.40	2.0
Veratraldehyde		>10000	<0.4
Guaiacol		>10000	<0.4
4-Ethyl-2-methoxyphenol		440.78	8.7
Catechol		>10000	<0.4
Tricaine methanesulfonate		>10000	<0.4
Benzocaine		>10000	<0.4
Tetracaine		>10000	<0.4
Propofol		>10000	<0.4

(L) of the light chain, measuring 1.9 Å, 2.2 Å, and 1.8 Å, respectively. It also forms a hydrogen bond with His91(L) of the light chain, which is 2.2 Å in length. The high number of hydrogen bonds may be one of the reasons for its high affinity with isoeugenol. Additionally, the *trans*-2-butenyl group of isoeugenol has a rigid structure that allows it to

maintain linearity and penetrate deeply into the docking pocket, creating hydrophobic interactions with Tyr32(H), which further enhances the binding activity between the antibody and isoeugenol.

Methyl isoeugenol has a structure similar to isoeugenol, with the only difference being a methoxy group at the fourth position of the

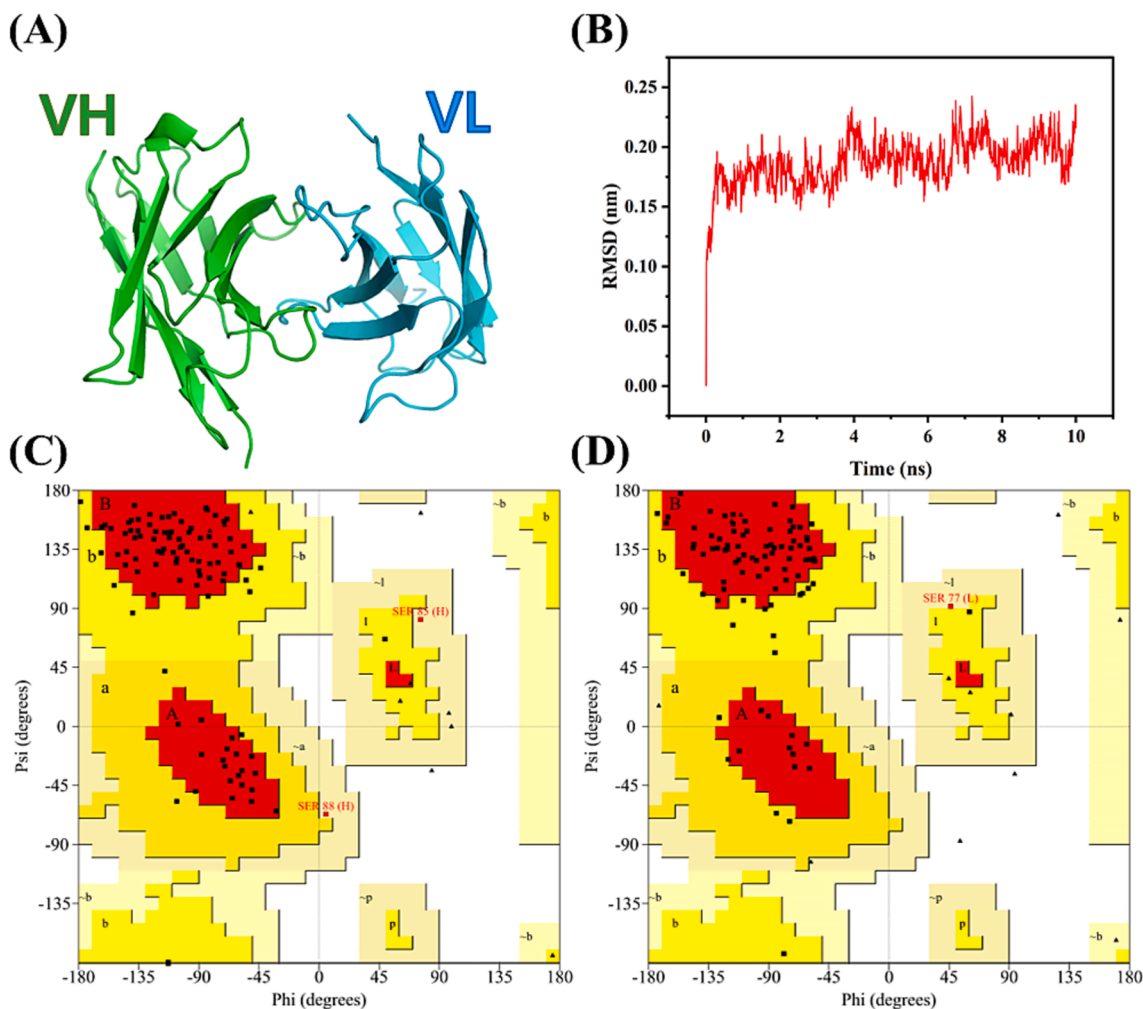


Fig. 5. (A) 3D model of Fv; (B) Dynamics RMSD plot; (C) Ramachandran plot of VH; (D) Ramachandran plot of VL.

phenyl ring, resulting in slightly lower binding activity than isoeugenol. From Fig. 6C1 and C2, it is apparent that its docking position and conformation are similar to isoeugenol's, but further analysis reveals that it forms three hydrogen bonds with the antibody, fewer than those formed by isoeugenol, and it cannot form a hydrogen bond with His91 (L). The main reason may be that the methoxy group of methyl isoeugenol, compared to the hydroxyl group of isoeugenol, has a larger steric hindrance, which is not conducive to the formation of hydrogen bonds.

Methyl eugenol, structurally similar to eugenol, exhibits significantly higher binding activity than eugenol does. Fig. 6D1 and 6D2 show that methyl eugenol forms three hydrogen bonds with Arg50(L), with lengths of 2.1 Å, 2.1 Å, and 1.6 Å, respectively, which is more than the number of hydrogen bonds formed between eugenol and the antibody. Additionally, the methoxy group at the fourth position on the phenyl ring of eugenol methyl ether is more hydrophobic than the hydroxyl group at the same position on eugenol. When the distance is too short to form hydrogen bonds, the longer-range hydrophobic interactions provided by the methoxy group could offer higher antibody binding activity, which may be one of the reasons for the higher activity of methyl eugenol compared to eugenol.

Acetyl isoeugenol, as depicted in Fig. 6E1, has its ester group surrounded by Phe32(L), Tyr92(L), and Tyr100(H), resulting in strong hydrophobic interactions. Moreover, acetyl isoeugenol forms three hydrogen bonds with Arg50(L), with lengths of 1.7 Å, 2.2 Å, and 1.8 Å respectively (Fig. 6E2). Although the substituent at the fourth position of its phenyl ring being an ester group, which has a larger molecular

volume, leading to significant steric hindrance, the number of hydrogen bonds it forms is greater than that of eugenol, this may make it has slightly higher binding activity than eugenol does.

To sum up, there are several factors that affect the binding activity between the anti-EUGs mAb and EUGs, including hydrogen bonding, hydrophobic interactions, and steric hindrance. Among these, hydrogen bonding plays a key role in the binding of antibodies to small molecules in the absence of significant steric hindrance. Additionally, Arg50(L) on the light chain is crucial for forming hydrogen bonds with the substituent groups on the phenyl ring of eugenol and its analogs, making it a key amino acid which can be the focus of in-depth study in subsequent directed molecular evolution for the development of anti-EUGs antibodies with better performance.

#### 4. Conclusion

In conclusion, three eugenol fragment-containing haptens with different carboxylic linkers in length were synthesized, and a broad-spectrum anti-EUGs mAb which can selectively bind with five EUGs with high-affinity was produced. By virtue of this mAb, a broad-spectrum ic-ELISA suitable for large-scale analysis five EUGs residue in aquatic products was developed, which exhibits both higher assay sensitivity and wider recognition spectrum for EUGs than previously reported immunoassays. Moreover, the molecular recognition mechanism for mAb-EUGs was studied by homology modeling and molecular docking, indicating that the numbers of the hydrogen bond formed between the EUGs and critical amino acids (Arg50(L) and His91(L)) in the

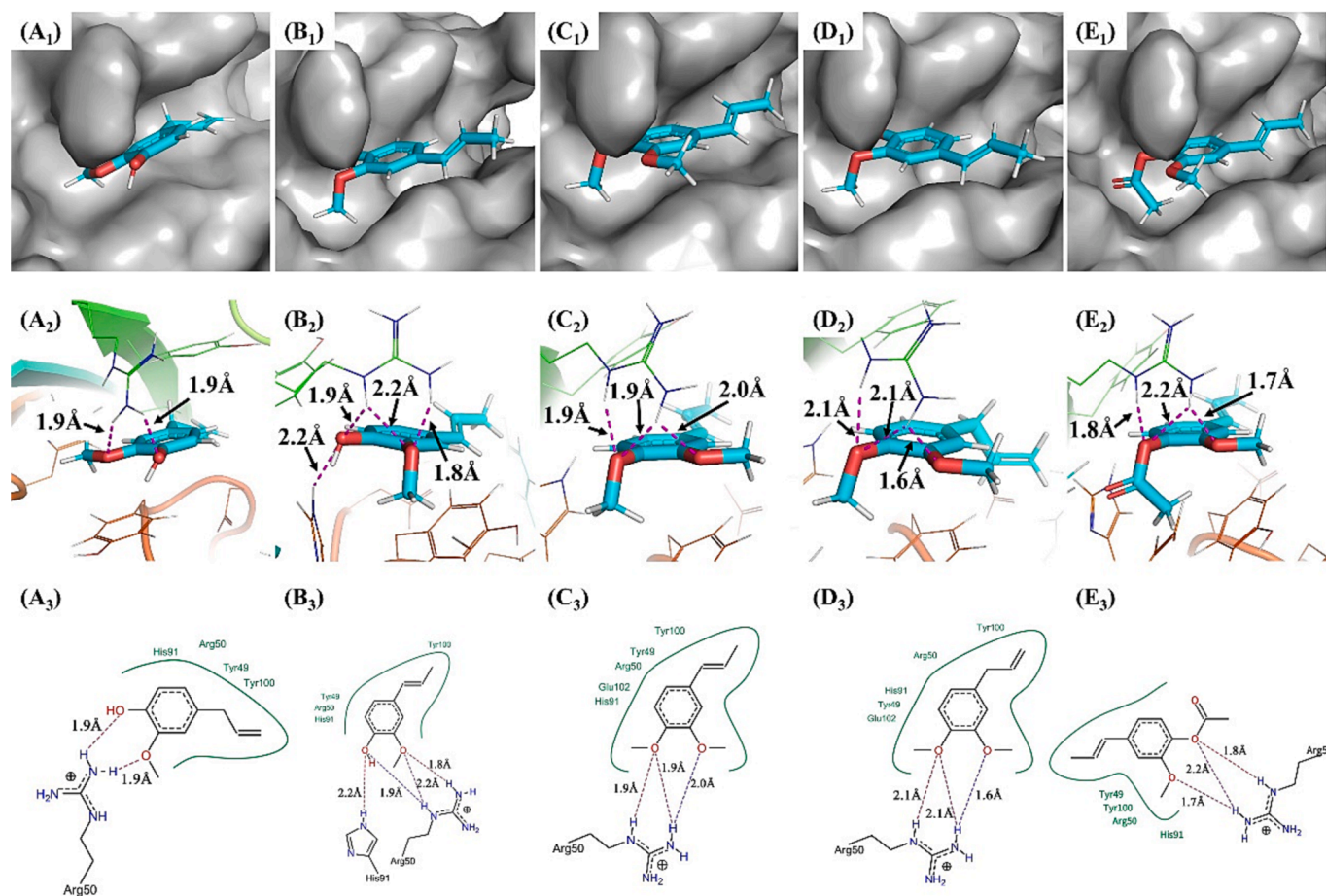


**Fig. 6.** The interaction between antibody and eugenol and analogues, the Purple dotted lines indicate hydrogen bonds; The compounds dock in the activity pocket of antibody (A<sub>1</sub>) Eugenol (A<sub>2</sub>) Isoeugenol (A<sub>3</sub>) Isoeugenol methyl ether (A<sub>4</sub>) Eugenol methyl Ether (A<sub>5</sub>) Acetyl isoeugenol; The three-dimensional image for docking (B<sub>1</sub>) Eugenol (B<sub>2</sub>) Isoeugenol (B<sub>3</sub>) Isoeugenol methyl ether (B<sub>4</sub>) Eugenol methyl Ether (B<sub>5</sub>) Acetyl isoeugenol; The two-dimensional image for docking (C<sub>1</sub>) Eugenol (C<sub>2</sub>) Isoeugenol (C<sub>3</sub>) Isoeugenol methyl ether (C<sub>4</sub>) Eugenol methyl Ether (C<sub>5</sub>) Acetyl isoeugenol. (For interpretation of the references to colour in this figure legend, the reader is referred to the web version of this article.)

variable region of the mAb predominantly determines the binding affinity. The study presents an effective approach for routine analysis of EUGs in aquatic products. Additionally, it serves as a useful reference for generating antibodies and developing immunoassays for diverse small molecular analytes.

#### Data availability statement

The datasets utilized in this study are available in online repositories. The specific names of the repository or repositories, as well as the corresponding accession number(s), can be found in the article or [Supplementary Materials](#).

#### Author contributions

Lin Luo: Conceptualization of the project, Formal analysis, Investigation, Methodology, Writing – review & editing. Rui-Yao Kang: Data curation, Investigation, Writing – original draft. Zhen-Xi He: Data curation, Investigation, Methodology. Bao-Zhu Jia: Data curation, Formal analysis. Zi-Jian Chen: Conceptualization, Methodology, Formal analysis, Foundation. Hao Deng: Funding Acquisition. Zhen-Lin Xu: Conceptualization, Investigation, Resources, Project administration.

#### Funding

This work was supported by Guangdong Basic and Applied Basic

Research Foundation (2021A1515012422, 2023A1515030011), the Heyuan Branch, Guangdong Laboratory for Lingnan Modern Agriculture Project (DT20220035), Guangzhou Planned Program in Science and Technology (202102021002), the Foundation for Distinguished Young Talents in Higher Education of Guangdong (2022KQNCX055), the “Climbing Plan” Project of Guangdong College Students Science and Technology Innovation Cultivation Special Fund (pdjh2022b0382). College Student Innovation and Entrepreneurship Training Program Project of South China Agricultural University (202239020227).

#### CRediT authorship contribution statement

**Lin Luo:** Writing – review & editing, Supervision, Project administration, Methodology, Funding acquisition, Formal analysis, Data curation, Conceptualization. **Rui-Yao Kang:** Writing – original draft, Methodology, Investigation, Formal analysis, Data curation. **Zhen-Xi He:** Writing – original draft, Methodology, Data curation. **Bao-Zhu Jia:** Writing – original draft, Investigation, Data curation. **Zi-Jian Chen:** Writing – review & editing, Methodology, Investigation, Formal analysis. **Hao Deng:** Writing – review & editing, Resources, Funding acquisition. **Zhen-Lin Xu:** Writing – review & editing, Supervision, Resources, Methodology, Formal analysis.

#### Declaration of competing interest

The authors declare that they have no known competing financial

interests or personal relationships that could have appeared to influence the work reported in this paper.

## Data availability

Data will be made available on request.

## Appendix A. Supplementary data

Supplementary data to this article can be found online at <https://doi.org/10.1016/j.fochx.2024.101255>.

## References

- Bai, Y., Liu, R., Dou, L., Wu, W., Yu, W., Wen, K., & Wang, Z. (2023). The influence of hapten spacer arm length on antibody response and immunoassay development. *Analytica Chimica Acta*, 1239. <https://doi.org/10.1016/j.aca.2022.340699>
- Dong, J., Li, Z., Wang, Y., Jin, M., Shen, Y., Xu, Z., & Sun, Y. (2021). Generation of functional single-chain fragment variable from hybridoma and development of chemiluminescence enzyme immunoassay for determination of total malachite green in tilapia fish. *Food chemistry*, 337, Article 127780. <https://doi.org/10.1016/j.foodchem.2020.127780>
- Dong, X., Liu, D., Meng, X., & You, T. (2022). Research progress on photoelectrochemical sensors for contamination analysis in agricultural fields. *Analytical Sciences*, 38(3), 459–481. <https://doi.org/10.2116/analsci.21SAR09>
- Fadillah, G., Wicaksono, W. P., Fatimah, I., & Saleh, T. A. (2020). A sensitive electrochemical sensor based on functionalized graphene oxide/SnO<sub>2</sub> for the determination of eugenol. *Microchemical Journal*, 159, Article 105353. <https://doi.org/10.1016/j.microc.2020.105353>
- Huang, Y. X., Li, Q., Zhang, Y. L., Meng, Z. J., Yuan, X. X., Fan, S. F., & Zhang, Y. (2021). Determination of six eugenol residues in aquatic products by gas chromatography-orbitrap mass spectrometry. *Journal of Food Quality*, 2021. <https://doi.org/10.1155/2021/9438853>
- Javahery, S., Nekoubin, H., & Moradlu, A. H. (2012). Effect of anaesthesia with clove oil in fish (review). *Fish Physiology and Biochemistry*, 38(6), 1545–1552. <https://doi.org/10.1007/s10695-012-9682-5>
- Ke, C., Liu, Q., Li, L., Chen, J., Wang, X., & Huang, K. (2016). Simultaneous determination of eugenol, isoeugenol and methyleugenol in fish fillet using gas chromatography coupled to tandem mass spectrometry. *J Chromatogr B Analyt Technol Biomed Life Sci*, 1031, 189–194. <https://doi.org/10.1016/j.jchromb.2016.07.048>
- Lei, X., Xu, X., Wang, L., Liu, L., Kuang, H., Xu, L., & Xu, C. (2023). Fluorescent microsphere-based lateral-flow immunoassay for rapid and sensitive determination of eugenols. *Food Chemistry*, 411, Article 135475. <https://doi.org/10.1016/j.foodchem.2023.135475>
- Li, J., Zhang, J., & Liu, Y. (2015). Optimization of solid-phase-extraction cleanup and validation of quantitative determination of eugenol in fish samples by gas chromatography-tandem mass spectrometry. *Analytical and Bioanalytical Chemistry*, 407(21), 6563–6568. <https://doi.org/10.1007/s00216-015-8823-y>
- Liang, H., Jia, B., Zhang, W., Wang, X., Zhou, K., Lei, H., & Luo, L. (2023). Ratiometric fluorescence immunoassay based on MnO<sub>2</sub> nanoflakes for sensitive and accurate detection of tricaine. *J Agric Food Chem*, 71(19), 7575–7583. <https://doi.org/10.1021/acs.jafc.3c00469>
- Lin, S., Jia, B., Luo, W., Wang, H., Lei, H., Zhang, W., & Luo, L. (2023). Controllable formation of polydopamine on carbon dots for ultrasensitive detection of alkaline phosphatase and ratiometric fluorescence immunoassay of benzocaine. *Food Chemistry*, 426, Article 136582. <https://doi.org/10.1016/j.foodchem.2023.136582>
- Luo, L., Lei, H., Yang, J., Liu, G., Sun, Y., Bai, W., & Xu, Z. (2017). Development of an indirect ELISA for the determination of ethyl carbamate in chinese rice wine. *Analytica Chimica Acta*, 950, 162–169. <https://doi.org/10.1016/j.aca.2016.11.008>
- Luo, L., Luo, S., Jia, B., Zhang, W., Wang, H., Wei, X., & Yang, J. (2022). A high-resolution colorimetric immunoassay for tyramine detection based on enzyme-enabled growth of gold nanostar coupled with smartphone readout. *Food Chemistry*, 396, Article 133729. <https://doi.org/10.1016/j.foodchem.2022.133729>
- Luo, L., Song, Y., Zhu, C., Fu, S., Shi, Q., Sun, Y., & Lin, Y. (2018). Fluorescent silicon nanoparticles-based ratiometric fluorescence immunoassay for sensitive detection of ethyl carbamate in red wine. *Sensors and Actuators B-Chemical*, 255, 2742–2749. <https://doi.org/10.1016/j.snb.2017.09.088>
- Luo, L., Wei, X., Jia, B., Yang, J., Shen, Y., Hammock, B., & Xu, Z. (2019). Modulating linker composition of haptens resulted in improved immunoassay for histamine. *Biomolecules*, 9(10), 597. <https://doi.org/10.3390/biom9100597>
- Ren, Z., Nie, B., Liu, T., Yuan, F., Feng, F., Zhang, Y., & Zhang, F. (2016). Simultaneous determination of coumarin and its derivatives in tobacco products by liquid chromatography-tandem mass spectrometry. *Molecules*, 21(11). <https://doi.org/10.3390/molecules21111511>
- Shen, X., Wu, X., Liu, L., & Kuang, H. (2019). Development of a colloidal gold immunoassay for the detection of four eugenol compounds in water. *Food and Agricultural Immunology*, 30(1), 1318–1331. <https://doi.org/10.1080/09540105.2019.1687658>
- Sun, P., Gao, Y. L., & Lian, Y. F. (2017). Determination of eugenol in aquatic products by dispersive solid-phase extraction and ultra-high-performance liquid chromatography-tandem mass spectrometry. *Food Analytical Methods*, 10(10), 3217–3224. <https://doi.org/10.1007/s12161-017-0882-6>
- Thompson, D. C., Barhoumi, R., & Burghardt, R. C. (1998). Comparative toxicity of eugenol and its quinone methide metabolite in cultured liver cells using kinetic fluorescence bioassays. *Toxicol Appl Pharmacol*, 149(1), 55–63. <https://doi.org/10.1006/taap.1997.8348>
- Vishruta Domlur Thyagaraj, R. K., Monica Kachroo, Anand S. Mayachari, Laxman P. Sawant, Murali Balasubramaniam. (2013). A validated RP-HPLC-UV/DAD method for simultaneous quantitative determination of rosmarinic acid and eugenol in Ocimum sanctum L. *Pharmaceutical Methods*, 4(1). <https://doi.org/10.1016/j.phme.2013.08.003>
- Zhao, X., Lei, C., Gao, Y., Gao, H., Zhu, S., Yang, X., & Wang, H. (2017). A ratiometric fluorescent nanosensor for the detection of silver ions using graphene quantum dots. *Sensors and Actuators B-Chemical*, 253, 239–246. <https://doi.org/10.1016/j.snb.2017.06.086>